ENVIRONMENTAL RESEARCH
LETTERS

LETTER • **OPEN ACCESS**

Street green space is relevant but not sufficient for adapting to growing urban heat in world cities

To cite this article: Giacomo Falchetta *et al* 2026 *Environ. Res. Lett.* **21** 084012

ENVIRONMENTAL RESEARCH
LETTERS

OPEN ACCESS

RECEIVED
16 December 2025

REVISED
5 March 2026

ACCEPTED FOR PUBLICATION
7 April 2026

PUBLISHED
23 April 2026

LETTER

Street green space is relevant but not sufficient for adapting to growing urban heat in world cities

Giacomo Falchetta[1,2,3,8,*], **Steffen Lohrey**[1,4,7,8,*], **Niels Souverijns**[5], **Dirk Lauwaet**[5], **Carl-Friedrich Schleussner**[1,6] and **Leila Niamir**[1]

[1] Energy, Climate, and Environmenty (ECE), International Institute for Applied Systems Analysis (IIASA), Laxenburg, Austria
[2] Centro Euro-Mediterraneo sui Cambiamenti Climatici (CMCC), Venice, Italy
[3] RFF-CMCC European Institute on Economics and the Environment, Venice, Italy
[4] Sustainability Economics of Human Settlements, Technische Universität Berlin, Berlin, Germany
[5] Flemish Institute for Technological Research (VITO), Mol, Belgium
[6] Integrative Research Institute on Transformations of Human-Environment Systems (IRI THESys) and the Geography Department, Humboldt-Universität zu Berlin, Berlin, Germany
[7] Current address: Institute for Environmental Studies (IVM), Vrije Universiteit Amsterdam, Amsterdam, The Netherlands
[8] Equal contribution.
[*] Authors to whom any correspondence should be addressed.

E-mail: falchetta@iiasa.ac.at and s.lohrey@vu.nl

Keywords: street green space, cooling potential, urban heat, urban green, climate change adaptation, scenario analysis, nature-based solutions

Supplementary material for this article is available online

Abstract

Cities face multiple growing climate-related risks. Identifying adaptation strategies and quantifying their effectiveness and limits is hence crucial. Street green space (SGS) receives significant attention in the urban heat adaptation space due to its potential to reduce heat load and provide additional ecosystem benefits. Yet, the majority of existing studies assessing the effectiveness of SGS are either global or very local, and typically rely on remotely-sensed surface temperature and green space density metrics. Limited evidence spanning across different urban and climate contexts exists. Here, we empirically estimate the heat stress reduction potential of SGS across global and local climate zones in 133 cities worldwide using air temperature and wet-bulb globe temperature (WBGT) daily outputs from UrbClim, a 100 m resolution urban microclimate model, combined with a high-resolution SGS indicator, the green view index (GVI). We quantify a SGS cooling efficiency interquartile range of $[-0.03, -0.01]$ $\frac{^{\circ}C}{GVI}$ for maximum WBGT, with substantial variation across global climate and local climatic zones. We design reality-bounded scenarios to explore possible evolutions of SGS until 2050. Combining these scenarios with the estimated cooling efficiencies, we show that ambitious yet locally feasible SGS expansion could offset 3%–11% (cities interquartile range) of the projected increase in maximum WBGT under a current policies climate change scenario, and 2%–7% under SSP5-(8.5), compared to a 2008–2017 climatology. These results highlight that SGS expansion is an effective yet insufficient strategy to adapt to the growing urban heat stress across cities worldwide. Conversely, reduced SGS from administrative inaction or climate impacts on vegetation health may worsen urban heat. These findings inform about the global adaptation potential and limits of urban street green, and can support policymakers in framing SGS expansion programs into a broader portfolio of actions to tackle growing urban heat and its adverse consequences.

1. Introduction

Heat is a major climate hazard, particularly in cities (Rohat *et al* 2018, 2019, Li *et al* 2025), where the majority of the human population lives (Dodman *et al* 2022) and the urban heat island effect (UHI) increases temperatures (Oke 1982, Liu *et al* 2020). Vegetation is an important nature-based solution (Wong *et al* 2021, Jiang *et al* 2025) against urban heat. It provides shading and latent cooling through

evaporation. Aerodynamically, vegetation increases the roughness length, increasing mixing with upper layers. Both effects generally lower temperatures, depending on moisture availability and neighbouring building height and density (Georgescu *et al* 2014, Wong *et al* 2021, Jiang *et al* 2025, Li *et al* 2025). Yet, substantial knowledge gaps remain on the extent to which vegetation along streets can reduce urban heat stress across highly different climates and urban forms (Klimenka *et al* 2025, de León *et al* 2025). Further, it is unclear whether expanding street-level vegetation to feasibility-bounded levels is sufficient for offsetting the additional heat projected under future climate change scenarios.

Street green space (SGS), defined as pedestrian-level vegetation along streets (Liu *et al* 2023), is a subcomponent of urban green space, focusing specifically on greenery that shapes human exposure in the public street environment. SGS has been shown to reduce street-level temperatures, even when accounting for other variables, e.g. sky-view factors (Chan *et al* 2024). Crucially, street-based SGS metrics may differ substantially from remote sensing measurements (Teeuwen *et al* 2024), in which typically larger areas such as parks and gardens can play a dominant role (Taubenböck *et al* 2021). Assessing the cooling potential of SGS is a complex research objective, since it is influenced by interactions of radiation and shading effects, differing albedos, materials' heat retaining capabilities and latent cooling through evapotranspiration, as well as vegetation impacts on aerodynamic roughness and thus wind speed (Rahman *et al* 2020). Shading—generally an important heat-reduction strategy (Turner *et al* 2023)—contributes the major share of cooling from trees (Shashua-Bar and Hoffman 2000), next to evapotranspiration (Li *et al* 2019, Rocha *et al* 2022). Vegetation provides further ecosystem and public health services, for example positive impacts on mental health (Lee and Maheswaran 2011, Nutsford *et al* 2013, Callaghan *et al* 2021). Importantly, cooling of the local microclimate also affects local morbidity and mortality (Gasparrini *et al* 2015, Friesen and Taubenböck 2025, Wang *et al* 2025, Wu *et al* 2025).

Estimates on the cooling efficiency (CE) of trees in cities—the sensitivity of a heat metric to the change in a vegetation metric—differ widely. Most differences depend on the type of metric used, especially surface or air temperature, but also the spatial scale studied (Lauwaet *et al* 2024), the urban form (Kirschner *et al* 2023), climate zones (Zhan *et al* 2024), or biomes (Rahman *et al* 2020, Wang *et al* 2020, 2022). In addition, study outcomes depend on whether all urban green areas—including parks or large backyards—or only SGSs are included. Most existing studies focus on the surface UHI (SUHI) (Voogt and Oke 2003, Tran *et al* 2006, Peng *et al* 2012, Zhou *et al* 2018, Mentaschi *et al* 2022) to assess urban heat effects, as this metric is easy to obtain from global remote sensing datasets. The SUHI is much larger in magnitude than the UHI for air temperature—within-city differences of 10–15 K have been reported for SUHI (Mentaschi *et al* 2022). In analogy, tree cooling efficiencies reported for surface temperature are also much larger in magnitude than those for air temperature (Du *et al* 2024). An overall CE of surface temperature by urban green between 1.5 °C and 5 °C has recently been suggested (Li *et al* 2024b), with low-density cities in the Global North showing much higher cooling through urban green. The CE is generally smaller in hot and humid climates than in drier ones (Wang *et al* 2020, Li *et al* 2024a).

Air temperature is typically a more appropriate metric for understanding heat load on humans than surface temperature (Budd 2008, Chakraborty *et al* 2021, Xiang *et al* 2023, Anders *et al* 2025), despite the large body of SUHI-based research. Thus, heat indices that include heat and radiation effects—such as the wet-bulb globe temperature (WBGT)—provide a more refined understanding of the heat mitigation potential of trees on the pedestrian scale. Fewer studies investigate such heat metrics, as they are more challenging to infer than surface temperature for urban microclimates (Anders *et al* 2025, Anders and Maronga 2025). Most studies report air temperature reductions by 1 °C−2 °C in parks (Shashua-Bar and Hoffman 2000, Bowler *et al* 2010) compared to the city, while *in-situ* measurements in direct vicinity to the tree have shown a reductions up to 11 °C in physical equivalent temperature (Rahman *et al* 2020). Much lower values are reported for larger scales, such as neighbourhoods, due to spatial averaging and decreasing CE with increasing distance from the tree canopy (Du *et al* 2024, Gobatti *et al* 2025). Indeed a spatial-scaling law for heat reduction analyses has recently been demonstrated: understanding local cooling efficiencies from small-scale investigations can be used to extrapolate to the city-wide cooling effect, with clear decreasing return (Wang *et al* 2024). Similarly, tree CE shows decreasing returns to density: the more trees are added to a non-vegetated area, the lower the additional cooling by each tree (Zhan *et al* 2024).

In this study, we conduct an evaluation of the role of SGS in reducing urban heat. We use air temperature and WBGT to assess heat, while considering a global pool of 133 cities across climate zones and urban forms. Our work provides a number of contributions to the literature: (i) first, it estimates heterogeneous cooling efficiencies of SGS at the neighbourhood-level based on granular microclimate data from the 100 m spatial resolution UrbClim urban climate model (De Ridder *et al* 2015, Souverijns *et al* 2026) and the green view index (GVI), a street-based indicator measuring SGS across 190 cities (Falchetta and Hammad 2025) worldwide. As opposed to the bulk of previous research, which mostly relies on greenness as seen from above, we use

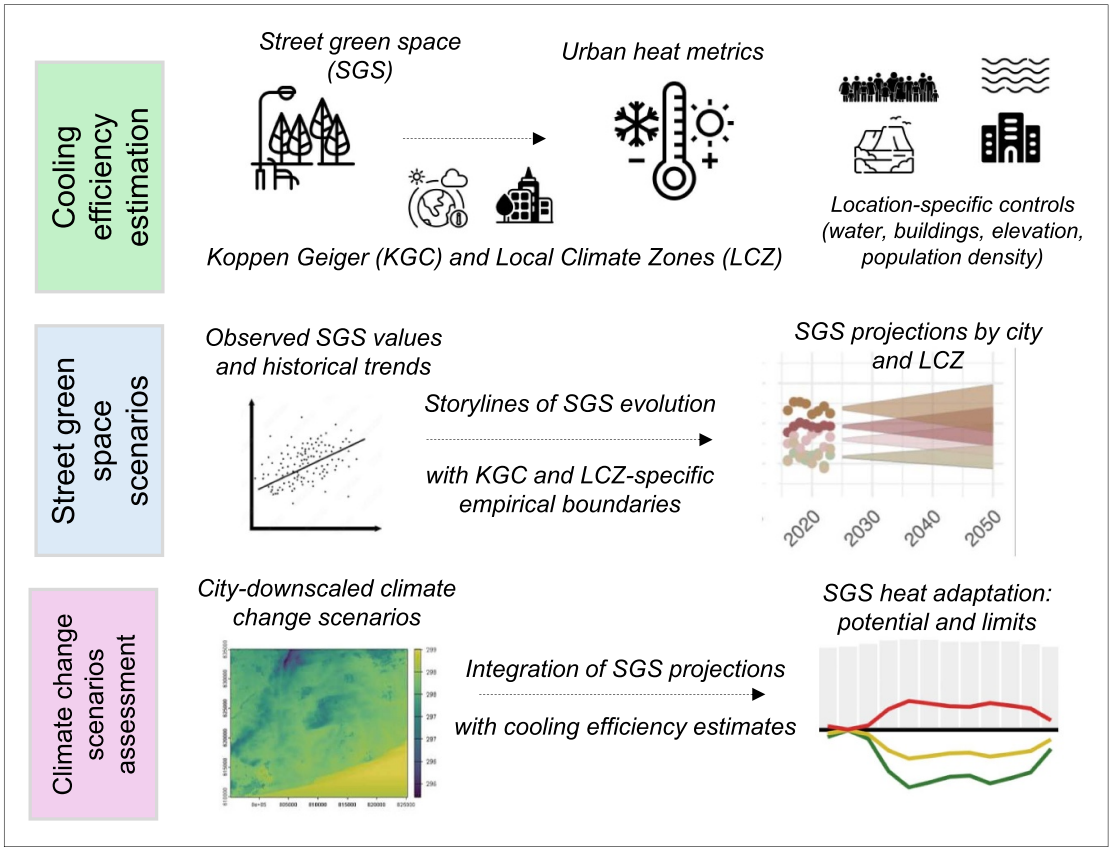

Figure 1. Schematic framework of the analysis of the role of street green space for urban heat mitigation conducted in this paper. Top row: empirical estimation of cooling efficiency coefficients; mid row: design and quantification of street green space scenarios; bottom row: evaluation of the joint role of climate change and street green space scenarios for urban heat.

estimates of street-level greenness. Also, our assessment benefits from the use of high spatio-temporal resolution urban climate model data, allowing to estimate air temperature and humidity, which have been show to yield significantly different estimates of CE compared to the prevalent use of remotely-sensed land surface temperature (Du *et al* 2024). (ii) Second, we introduce and develop a set of scenarios for potential future evolutions of SGS (Massaro *et al* 2023), contributing to the literature that calls for new quantitative research to bridge the scale between the local particular and the global universal in climate change assessments of cities (Creutzig *et al* 2025). (iii) Third, based on our estimates of cooling efficiencies and these SGS city-level projections, we evaluate the future cooling potential of SGS expansion and thus reduce local heat-related exposure in the face of projected climate change by 2050, referring to four global climate change scenarios from the PROVIDE project (Lamboll *et al* 2022).

Our study thus contributes to the growing strand of research quantifying the effectiveness and limits of adaptation strategies against climate change impacts (Juhola *et al* 2024, Callahan 2025, Puig *et al* 2025). The workflow of the analysis is schematically represented in figure 1. Our findings inform the design of climate-resilient cities and the reduction of maladaptive risks by shedding new light on the heterogeneous efficiency of SGS expansion as a strategy to tackle growing heat stress across different global to local climate zones (LCZ).

2. Materials and methods

2.1. Urban climate model data

The urban microclimate data is obtained from the UrbClim mesoscale climate model (De Ridder *et al* 2015) for urban applications. UrbClim is an urban boundary layer model that calculates meteorological output variables, such as air temperature, humidity and land surface temperatures, and allows the computation of urban climate for entire cities. It is able to downscale large-scale meteorological inputs (in this case ERA5) to high spatial detail by using detailed urban boundary layer physics and a high-resolution description of the land use characteristics obtained from satellites. The land use parameters that are considered by UrbClim encompass land cover, imperviousness, building fraction and height, NDVI, anthropogenic heat fluxes, and soil texture. Model setup and input data are detailed in Souverijns *et al* (2026).

UrbClim has a spatial resolution of 100 m, meaning that atmospheric and surface processes are resolved at the neighbourhood scale, with each grid cell representing average conditions over an area of approximately one hectare. Its outputs are available hourly for a 10 year historical period (2008–2017). Our analysis is based on daily values of the variables considered. In this study, we select 133 cities worldwide (Lauwaet *et al* 2024), which are part of the PROVIDE project (Lamboll *et al* 2022) and for which validated UrbClim output exists (Souverijns *et al* 2026). Maps of these cities with their climate zones (figure SI-1) and a schematic illustration of their urban morphology (figure SI-3) can be found in the appendix.

We use surface air temperature T_a and wet-bulb globe temperature T_{wg} to understand the cooling role of SGS. We consider daily mean, maximum, and minimum values for both metrics. T_a is a universal metric, but its ability to describe heat load on humans is limited. T_{wg} is a more appropriate heat indicator for this purpose (Yaglou and Minard 1957, Kong and Huber 2022), as it captures the joint effects from air temperature, relative humidity, wind speed and solar radiation effects. The UrbClim model results for all considered cities have been validated against meteorological observations from NOAA, providing limited biases (Souverijns *et al* 2026). It must be noted that this validation is limited to rural stations. Within different projects, we also executed validation against urban meteorological measurements. This has been executed for both European (Bilbao, Toulouse, Antwerp, Barcelona, Brussels, London) and non-European (Colombo, Niamey and Johannesburg) cities, showcasing in general an accurate representation of the urban climate (De Ridder *et al* 2015).

2.2. Climate change scenarios

We include climate change impacts by using four scenarios from PROVIDE[9] (Lamboll *et al* 2022): *2020 climate policies* (temperature consistent with 2020 submitted Nationally Determined Contributions); *delayed climate action* (deep decarbonisation occurring from the 2030 s); *shifting pathway* (stringent climate policy to stay well below 1.5°, although with possibility of an overshoot); and *SSP5-8.5*.

2.2.1. Future heat variables

Instead of forcing the UrbClim model with different realisations of future climate, which would be computationally expensive, the quantile delta mapping algorithm is applied (Olsson *et al* 2009, Willems and Vrac 2011). This method calculates future changes in different parameters (i.e. air temperature, humidity and land surface temperature) relevant in the computation of the WBGT. These delta values are obtained from a set of MESMER-M climate emulations (Souverijns *et al* 2026). This provides average monthly difference (deltas) between future values and the values for the historical climatological period for each city and scenario in 10 year intervals. By combining these results with CMIP6 daily values, also changes in different temperature quantiles (i.e. extreme temperatures generally change with higher amounts than average temperatures) are considered. This approach has been proven to work for the climatological time-scale in Lauwaet *et al* (2015) and is explained in detail in section 4 of Souverijns *et al* (2026). The delta changes are applied in the following way:

$$T_{a,\text{future}} = T_a + \Delta T_a. \tag{1}$$

For historical years, UrbClim computes T_{wg} following the iterative approach by Liljegren *et al* (2008), Souverijns *et al* (2026). For future years, we use a modified version of the seminal equation by Yaglou and Minard (1957) to compute $T_{wg,\text{future}}$:

$$\begin{aligned} T_{wg,\text{future}} = {} & 0.7\ T_{w,\text{future}} + 0.2\ (T_s + \Delta T_s) \\ & + 0.1\ (T_a + \Delta T_a). \end{aligned} \tag{2}$$

For this approach we require the future wet bulb temperature $T_{w,\text{future}}$ which we obtain by using the analytical equation by Stull (2011), valid for most relevant regimes of T and RH at standard sea-level pressure:

$$\begin{aligned} T_w = {} & T_a \operatorname{atan}\left[0.151\,977\ (RH + 8.313\,659)^{\frac{1}{2}}\right] \\ & + \operatorname{atan}(T_a + RH) - \operatorname{atan}(RH - 1.676\,331) \\ & + 0.003\,918\,38\, RH^{\frac{3}{2}} \operatorname{atan}(0.023\,101\ RH) \\ & - 4.686\,035 \end{aligned} \tag{3}$$

where T_a is dry bulb temperature in °C and RH is relative humidity in %[10]. Mean relative humidity RH for historical years can be derived from mean specific humidity and the pressure at a city's elevation:

$$RH = 26.3\, p\, q \exp\left[-\frac{17.67\ (T_a - 273.15)}{(T_a - 29.65)}\right] \tag{4}$$

where p is air pressure and q specific humidity[11]. When $T_w = f(T,\ RH)$, and with only RH_{mean} available for future runs, we obtain:

$$T_{w,\text{future},x} = f(T_x + \Delta T_x,\ RH_{\text{mean}} + \Delta RH_{\text{mean}}), \tag{5}$$

where $x \in \{\text{mean}, \text{min}, \text{max}\}$. In analogy, and using equation (2):

[9] https://climate-risk-dashboard.iiasa.ac.at/keyconceptsscenario-list.

[10] We compared the outcomes against the psychometric equations provided by the *R psychrolib* package, which is based on the ASHRAE equations taking into account pressure, and the error from non-sea level pressure also for higher elevations appeared small.

[11] We use mean air pressure for the city's altitude from hypsometric equation using the `bigleaf` (Knauer *et al* 2018) *R* package.

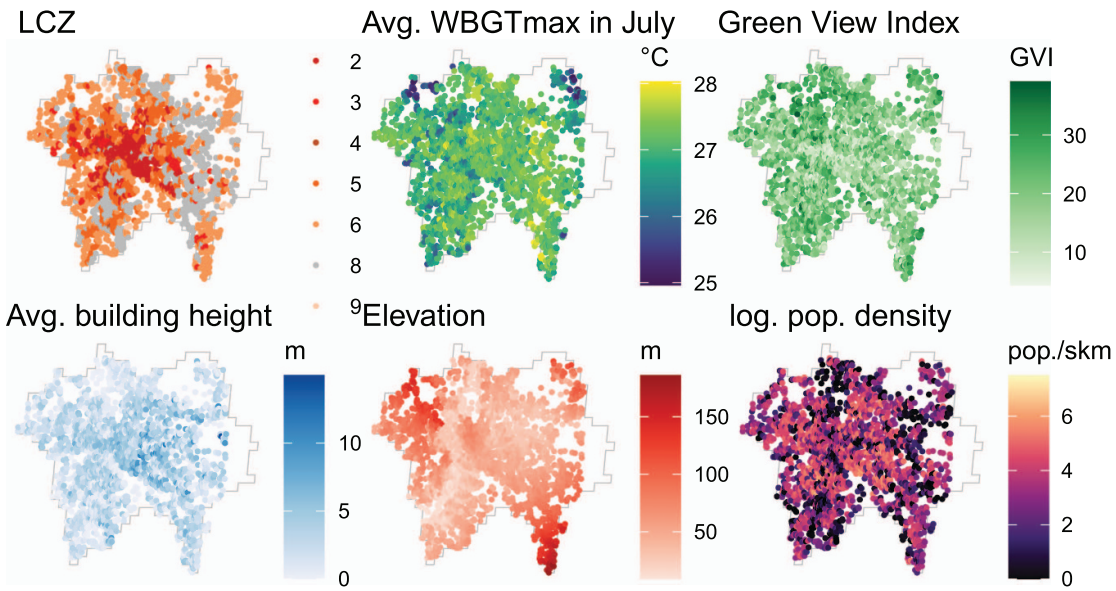

Figure 2. Schematic visualization of selected variables in the assembled sampling point-level dataset for the functional urban area of Rome, Italy.

$$T_{wg,\text{future},x} = f(T_{w,\text{future},x},\ T_{s,x} + \Delta T_{s,\text{mean}},\ T_{a,x} + \Delta T_{a,\text{mean}}). \quad (6)$$

We use $\Delta T_{s,\text{mean}}$ in all future runs also for $T_{s,\text{min}}$ $T_{s,\text{max}}$.

2.3. SGS data and local co-variates

2.3.1. SGS dataset

To derive the local SGS density, we rely on the GVI, a street vegetation canopy cover density metric ranging from 0 to 100. We leverage the dataset produced by Falchetta and Hammad (2025), which provides validated estimates of the GVI for each of the 133 cities covered by our analysis. Such estimates are produced by estimating GVI values in a large pool of 10 m-buffered sampling points within the urban boundaries of each city in each year between 2016–2023. This approach, described in detail in Falchetta and Hammad (2025), leverages a machine learning (ML) model trained with multispectral remotely sensed data as well as several climatological variables from ERA5 to estimate coordinate point-level GVI values. The model is trained on ground-truth provided by Seiferling *et al* (2017), who calculate coordinate point-level GVI using google street view imagery for a pool of world cities. Table SI-4 describes the distribution of the estimated SGS levels for each of the 133 cities covered by our analysis, stratified by LCZ. In this sense, the GVI metric is an estimate of greenness as 'seen by the pedestrian'. It does however not distinguish either between different species, or vegetation types (e.g.trees and bushes or grassy areas), or irrigated vs. non-irrigated urban green.

2.3.2. Urban form and Köppen-Geiger climate (KGC) zones

We assign LCZ and KGC classifications to each sampling point and city. KGC provides an established way to represent general climate zones (Peel *et al* 2007). We use the main climate zones tropical (A), arid (B), temperate (C), and continental (D). The LCZ characterizes the local urban built environment according to buildings' height and sparsity (Stewart and Oke 2012, Demuzere *et al* 2022). Throughout the paper, we also refer to LCZ as *urban form*.

2.3.3. Additional spatial covariates for regression analysis

For each sampling point containing information on the local value of GVI and of heat metrics, we introduce additional information on factors potentially affecting heat metrics: the average buildings height from the GHS-BUILD-H product (Florczyk *et al* 2019a), a binary variable indicating the presence of water bodies (European Union Copernicus Land Monitoring Service Information 2022), the average terrain elevation from the Amazon Web Services Terrain Tiles (2025), and the local population density from the Global Human Settlement Layers GHS-POP product (Florczyk *et al* 2019b). The resulting dataset upon which the analysis is conducted is depicted in figure 2 for the functional urban area of Rome, Italy.

2.4. SGS future scenarios

We develop three different scenarios to explore plausible futures of SGS. These scenarios are based on observed lower and upper bounds across the entire dataset, stratified by LCZ and climate zone KGC

Table 1. Assumptions for different SGS scenarios. Reference SGS refers to the Universe of SGS observations for the corresponding LCZ / KGC combination.

Scenario	Percentile	Description
Decreased Provision	25th	Decrease of current vegetation median to 25th percentile of reference SGS
Moderate Ambition	75th	Assumes growth of SGS to the 75th percentile of reference SGS.
High Ambition	90th	Assumes growth of SGS to the 90th percentile of reference SGS.

(table 1). We use the median (50th percentile) of the historical observations (2016–2023) across each observation point as baseline level of street green. The historical SGS observations show year-to-year variations, largely reflecting inter-annual weather variability rather than structural changes in urban green infrastructure (Falchetta and Hammad 2025). We define plausible upper and lower limits of urban greening by using the observed variation across all observed points. Specifically, we use the 90th and 10th percentile of all point-based SGS observations for each LCZ and KGC (figure SI-15), respectively. The resulting statistics shows that lower limits of SGS are comparable across climate zones and land cover zones, with totals in open and sparse settlement patterns larger than in more compact urban forms. Upper limits however depend more strongly on climate zones; the maximum observed SGS in dry KGCs is much lower than in tropical climates, temperate or continental ones (also see figures SI-16 and SI-17 in the supporting information.)

From these assumptions and observational inputs, we develop three scenarios of SGS development from the present to 2050: (*Decreased Provision*), *Moderate Ambition* and *High Ambition* (table SI-5). In the Decreased Provision scenario, we assume declining urban green to the 25th percentile of all observed 2016–2023 values within the corresponding KGC and LCZ combination and all cities in the analysis. This mirrors adverse climate change impacts on urban vegetation health (Esperon-Rodriguez *et al* 2024). In the Moderate Ambition scenario, we model the growth of SGS to the 75th percentile of the corresponding KGC and LCZ combination, and to the 90th percentile for the High Ambition scenario.

Figure 3 illustrates the three scenarios of SGS for three selected LCZs in Vienna, Austria. Furthermore, figure SI-17 in the appendix shows the distribution of scenarios across all cities covered by our analysis, and projected values can be found in table SI-5.

2.5. Estimation of heterogeneous cooling efficiencies

Cooling efficiencies are estimated through city-specific fixed effects regression models of SGS on urban heat metrics produced by the UrbClim urban microclimate model (De Ridder *et al* 2015, Lamboll *et al* 2022), with a spatial resolution of 100 m and a daily temporal resolution. Using sampling points in each of 133 cities and taking into account the city-specific KGC zone, as well as location-specific urban form (LCZ), the empirical strategy relies on spatio-temporal variation in local climate conditions.

In UrbClim, greenness is derived from MODIS & Landsat NDVI images in the form of monthly averages for the 2008–2017 period, while GVI is aggregated as the median value across all available years (2016–2023) to capture persistent street-level greenness patterns. The temporal mismatch between the two is not a concern due to the focus on cross-sectional within-city spatial variation in GVI of the regression models, as well as the fact that the observation period-median GVI provides a reasonable proxy for long-run street greenness at each location[12], consistent with the spatial scale and climatological nature of the heat metrics considered.

2.5.1. Fixed-effects regression analysis

To estimate within-city spatial associations between SGS and heat indicators in each LCZ while accounting for observed local characteristics, we estimate a pool of spatially-granular regression models at the sampling point-level within each of the 133 cities covered by our analysis. Specifically, we estimate city- and LCZ-specific regression models using a two-way fixed-effects (month and year) specification of the following functional form:

$$HM_{ilcmt} = \mathrm{SGS}_{ilc} \times \mathrm{month}_m + \zeta_{ilc} + \mathrm{month}_m + \mathrm{year}_t + \epsilon_{ilcmt} \quad (7)$$

where, for each sampling point i, LCZ l, city c, month m, and year t, HM is—depending on the specification—a heat metric; month is a categorical variable for each of the 12 months of the year; SGS is the continuous variable measuring the GVI index of the density of SGS, ζ is a vector of sampling point-specific time-invariant co-variates (including building heights, population density, water bodies presence, and elevation). Hence, for each city and LCZ existing in that city, the regression models seek to evaluate month-specific marginal association between SGS and HM, rather than an average city-wide or year-round effect.

We also estimate a set of LCZ-specific pooled specifications that combine sampling points from all

[12] The inter-annual variation in GVI is largely driven by image acquisition timing and weather-related phenology rather than by structural changes in urban tree stock (Falchetta and Hammad 2025).

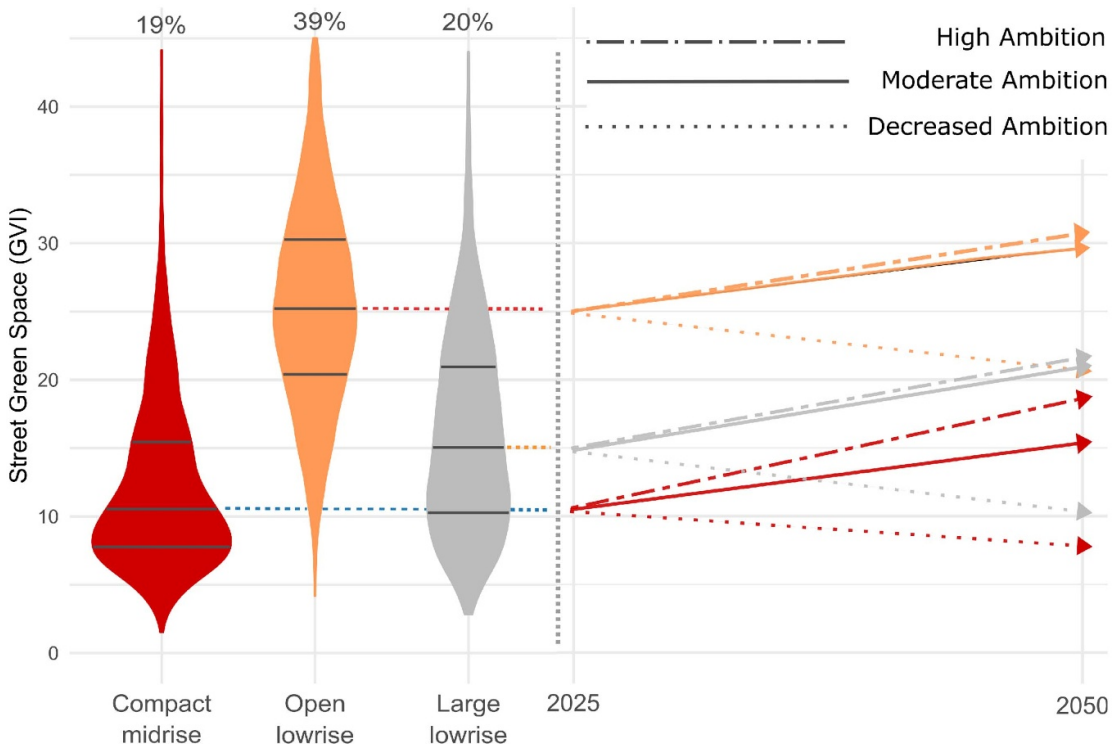

Figure 3. Illustrative example of the scenarios of street green space (SGS) evolution in Vienna, Austria for three important land cover zones. Percentages give the relative occurrence of each LCZ over the total city area. The violin plots represent the distribution and median values of the inter-annual variability in the historical observed SGS (2016–2023). Horizontal lines separate quartiles. We use the median as baseline. Moving towards 2050, the dashed, dotted, and dash-dotted lines illustrate the Decreased Provision, Moderate Ambition, and High Ambition scenarios, respectively.

cities, adding city-by-month and city-by-year fixed effects to control for city-specific seasonality and interannual variation in *HM*, and hence estimating average LCZ-specific marginal associations across the entire pool of cities covered by the analysis:

$$HM_{ilcmt} = \mathrm{SGS}_{ilc} \times \mathrm{LCZ}_{ilc} + \zeta_{ilc} + \mathrm{city}_c \cdot \mathrm{month}_m + \mathrm{city}_c \cdot \mathrm{year}_t + \epsilon_{ilcmt}. \quad (8)$$

Finally, we also conduct a set of robustness tests on the pooled sample—described and reported in the SI Append (tables SI-6–SI-23).

Note that a causal interpretation of the estimated coefficients would require strong additional assumptions. First, conditional on the included covariates and month and year fixed effects, SGS would need to be as-good-as randomly assigned across sampling points (no unobserved confounding factors). Second, the functional form would need to be correctly specified (including any relevant non-linearities and interactions). Third, measurement error in SGS and heat metrics would need to be limited or at least not systematically correlated with omitted determinants. Finally, spatial spillovers would need to be negligible at the scale of analysis; in practice, cooling from vegetation can propagate beyond the immediate pixel, and the 100 m UrbClim resolution implies that each observation already represents spatially averaged conditions rather than micro-scale role of individual trees. In our analysis for brevity, we retain the term "CE" as commonly used in the urban climate literature, while emphasising that our estimates are best interpreted as conditional spatial associations.

2.5.2. Cooling efficiencies calculation

We use the outcome regression coefficients to calculate the LCZ- and month-specific CE of SGS. CE quantifies the extent to which a given area of green spaces in a city can reduce temperatures. Although there is no standard accepted definition, it is measured as the slope or the functional form of the relationship between temperature and vegetation cover through regression analysis (Li *et al* 2024a), after correcting for those confounding factors. In a context of linear modelling, *CE* can be expressed as the marginal response of a heat indicator *HM* as measured in month *t*, in city *c* and in LCZ *l* from a marginal change in SGS:

$$\mathrm{CE}_{clm} = \frac{\partial HM_{clt}}{\partial \mathrm{SGS}_{cl}}. \quad (9)$$

Note that in a context of non-linear modelling, C E is not a constant, but it will be expressed as a function of the level of SGS, hence for any given level x of SGS, it will be given by $\frac{\partial f(HM,\mathrm{SGS}=x)}{\partial \mathrm{SGS}}$.

2.5.3. Calculation of heat metrics change in SGS and climate change scenarios

To calculate the change in each heat metric *HM* in each climate change scenario, LCZ, month, SGS scenario, and year, we estimate the following:

$$\Delta HM_{clmst} = \mathrm{CE}_{clm} \cdot (\mathrm{SGS}_{clt} - \mathrm{SGS}_{clt=2020}). \quad (10)$$

The net average city-level effect is obtained by weighting the estimated temperature change values by the share of urban area covered by each LCZ class *l* and aggregating:

$$\Delta HM_{cmst} = \sum HM_{cmlst} \cdot \mathrm{share}_{clst}. \quad (11)$$

Finally, it is possible to derive the temperature reduction potential of increasing SGS as:

$$\mathrm{offset}_{cmst} = -\frac{\Delta HM_{cmkt}}{\Delta CC_{cmst}} \quad (12)$$

where ΔCC_{cmkt} are the projected impacts of anthropogenic climate change on heat metrics in every city *c*, month *m*, climate change scenario *k*, and year *t*.

3. Results

3.1. SGS: CE by climate zone and urban form

We show estimates of the cooling efficiency (CE), i.e. the change of a heat metric in response to a change in SGS. We focus on results for maximum wet-bulb globe temperatu $T_{wg,\max}$, as this is arguably the most relevant metric for heat exposure. SGS-specific cooling efficiencies are plotted by KGC and LCZ (figure 4), and also binned by temperature (figure 5). These cooling efficiencies are based on the city-specific regression models, which are preferred over regression models pooling together data from all cities due to their aptness to account for city-specific features affecting the relation of interest. Supplementary regression tables displaying results for specifications estimated on the pooled cities sample are found in tables SI-6–SI-23. Results for additional heat metrics—minimum, mean, and maximum daily values for T_{wg} and 2m air temperature T_a—are shown in the appendix (figures SI-4–SI-8). Figures SI-13–SI-10 show the same results, but only including CE coefficients which are statistically different from 0[13].

Across the two different metrics analysed, we find that SGS is most effective in decreasing $T_{wg,\max}$ and $T_{a,\min}$. The strong cooling role for $T_{a,\min}$ likely reflects evapotranspiration and shading effects, which reduce heat storage in concrete and stone surfaces during the day and limit nocturnal heat release. In contrast, for some combinations of LCZ and climate zone, we observe small positive coefficients for $T_{a,\mathrm{mean}}$ and $T_{a,\max}$ (figures SI-12 and SI-13), indicating a warming association, although positive coefficients are typically smaller in magnitude and less frequently statistically significant than negative ones. The estimated cooling efficiencies for $T_{wg,\max}$ are predominantly negative (IQR: $[-0.03, -0.01]$ °C), with a mean of -0.026 °C and a median of -0.019 °C. A *t*-test shows both differ statistically from zero ($p < 0.01$), highlighting the largely prevalent heat stress reduction role of SGS. This implies, for example, that a 10-point increase in the local GVI would correspond to a reduction of roughly 0.1–0.3 °C in $T_{wg,max}$. Higher temperatures show larger cooling efficiencies overall for $T_{wg,\max}$ (figure 5), as well as for $T_{wg,\min}$ (figures SI-5 and SI-11) and $T_{wg,\mathrm{mean}}$ (figures SI-4 and SI-10). Cooling efficiencies are generally larger in dry and continental climates and smaller in temperate climates. In some LCZs and months, SGS is associated with a warming effect. This is most prominent in tropical and continental climates and in compact urban forms, which also show a wide dispersion of coefficients (figure 4). Similar patterns are found for air temperature, for example for maximum air temperature in sparsely built LCZs and compact high-rise zones (figure SI-2). When binning coefficients by $\bar{T}_{wg,\max}$ (figure 5), the strongest cooling occurs when $T_{wg} > 30$ °C. Further differentiation by climate zone (figure SI-3) shows that the increase in CE with average temperature is most pronounced in temperate and tropical climates, and less so in dry ones.

The physical mechanisms underlying these heterogeneous effects are multiple. Vegetation cools by shading surfaces, thereby reducing absorbed shortwave radiation, and by evapotranspiration, which partitions incoming energy into latent rather than sensible heat flux. The latter reduces air temperature but increases humidity. Because T_{wg} incorporates both air temperature and humidity, this dual effect partly explains why cooling efficiencies differ between T_a and T_{wg}. Vegetation also modifies the aerodynamic properties of the urban boundary layer. Trees increase surface roughness, potentially reducing wind speed while enhancing turbulent heat exchange. In low-rise and sparsely built areas, higher roughness lengths may partly counteract radiative and evaporative cooling, contributing to the lower or even positive coefficients observed in some LCZs (figure 4). All these processes, including shading, moisture availability, and aerodynamic interactions, are represented in the UrbClim model.

For air temperature $T_{a,\min}$, $T_{a,\mathrm{mean}}$, and $T_{a,\max}$, cooling is most pronounced in dry and tropical climates (figures SI-6–SI-8). In temperate climates, several LCZ combinations show small or statistically insignificant effects when excluding non-significant estimates (figures SI-12–SI-14). Continental cities display largely insignificant coefficients for T_a. The

[13] We decided to show all results—including statistically insignificant coefficients—in the main part of the paper, as lack of statistical significance is a result in itself, implying that a null effect for the CE for a given context can be found.

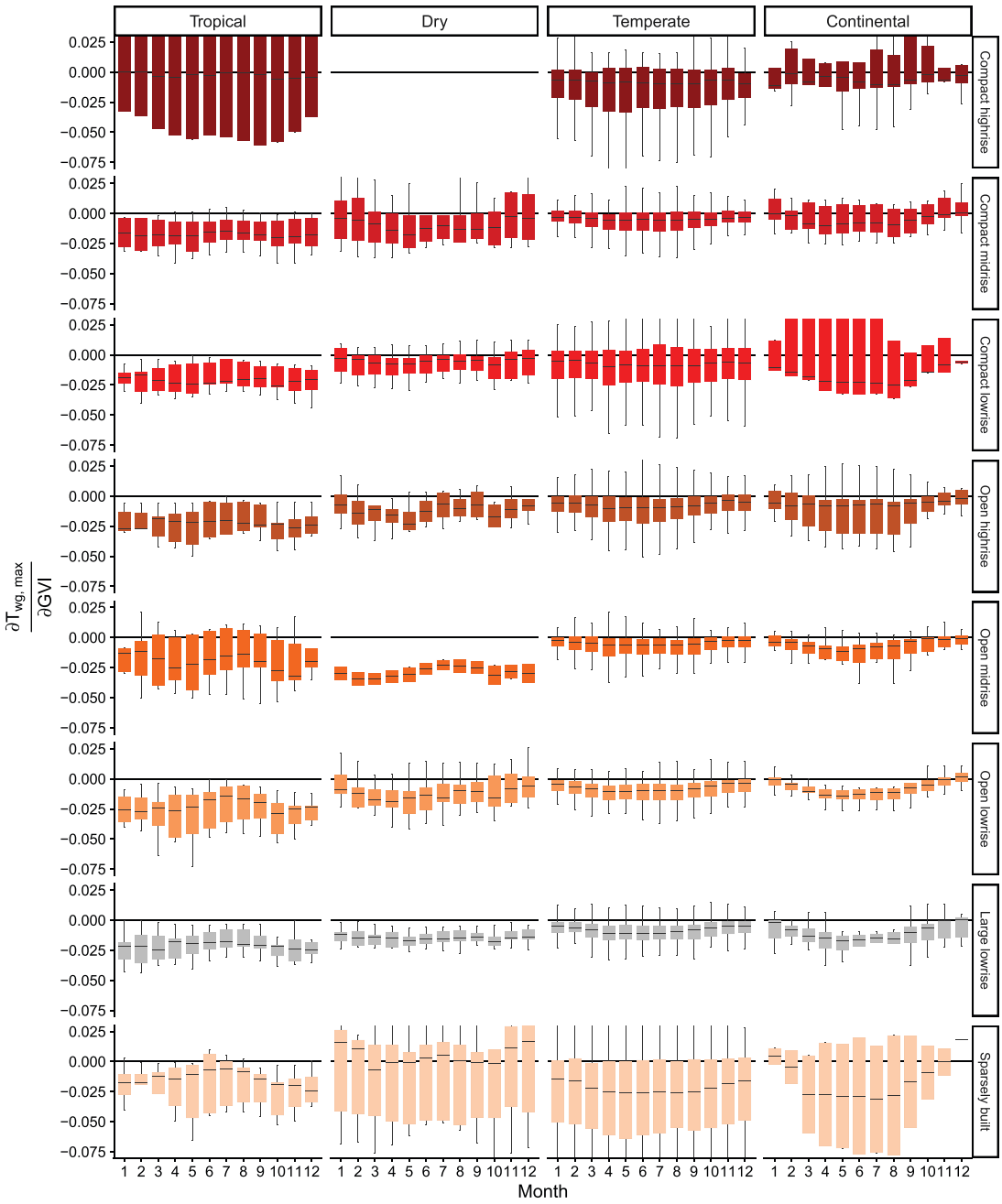

Figure 4. Distribution of the empirically estimated street green space cooling efficiency coefficients for $T_{wg,\max}$ across 133 global cities, by Köppen-Geiger climate zones (columns) and local climate zones (rows). Each coefficient expresses the expected change response in $\mathbf{T_{wg}}$ in response to a one-unit increase in GVI, the SGS metric adopted in this study. Values for other metrics are reported in the SI appendix.

increase of CE with increasing temperature is less systematic for T_a than for T_{wg}. In some temperate LCZs, binning by $T_{a,\max}$ suggests increasing CE at higher temperatures (figure SI-2), although part of this pattern may reflect binning artefacts.

SGS shows the strongest cooling coefficients in open and large low-rise urban forms, with effects more pronounced for T_{wg} than for T_a. Sparsely built zones display larger variability, while compact land-use classes show smaller average cooling efficiencies. CE is generally smaller in areas with lower baseline temperatures, particularly in temperate and continental climates, where moisture availability and seasonal dynamics vary more strongly. It should also be noted that our sample contains a larger number of temperate cities than other climate zones.

3.2. SGS: effectiveness and limits to reduce future heat

A core policy question concerns the extent to which increasing urban green—including SGS—can reduce future additional heat from climate change. Figure 6

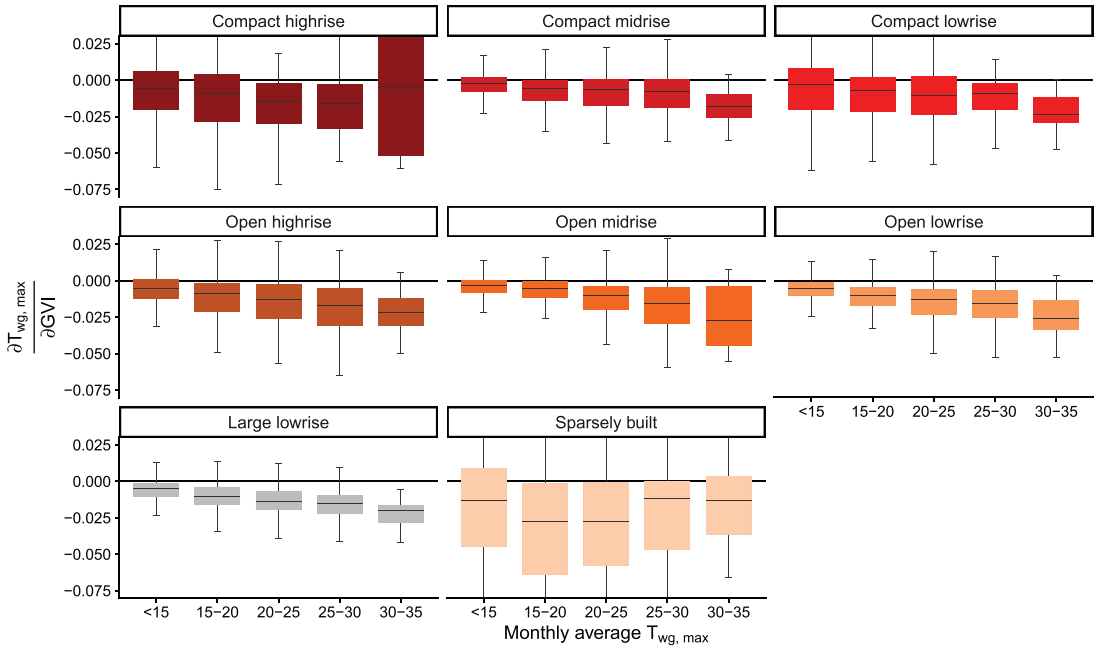

Figure 5. Distribution of the empirically estimated street green space cooling efficiency coefficients for $T_{wg,\max}$ across 133 global cities, by $T_{wg,\max}$ interval and local climate zones (facets). Each coefficient expresses the expected change response in $T_{wg,\max}$ in response to a one-unit increase in GVI, the SGS metric adopted in this study.

shows the projected magnitude of climate change impacts on daily $T_{wg,\max}$ around 2050, with the distribution of each box plot expressing model uncertainty across 25 GCMs, on the left hand side. The estimated cooling benefit of the three SGS scenarios is then shown on the right hand side of each panel for a pool of four selected cities in different regions and macro-climatic zones. Similar figures for other heat metrics shown in the appendix (figures SI-18–SI-22). Table SI-24 provides city-level projected heat stress change for all cities, heat metrics, climate change scenarios and SGS scenarios, and results described below can be found in that table.

We find that climate change will increase city-scale heat stress significantly across the majority of cities covered by our analysis. For daily $T_{wg,\max}$, we find that under a current climate policies scenario, the heat metric will on average (across all days of the year and inclusive of the range of uncertainty from 25 GCMs) increase by 0.97 °C (IQR: [0.43–1.52] °C), growing up to 1.7 °C (IQR: [1–2.3] °C) in a SSP5-8.5 scenario. Exceptions include some cities (e.g. Tehran or Addis Ababa) where irrespective of increasing temperatures, projected decreases in humidity may decrease T_{wg} in certain periods of the year. Looking at SGS scenarios impact on T_{wg}, we find that such potential is strongly dependent not only on the scenario, but also on the specific city. Cities where SGS expansion might lead to the strongest cooling benefit in terms of daily maximum T_{wg} absolute reduction include Bogota, Dhaka, Mexico City, Reykjavik and Nairobi. On the other hand, major cities where the High Ambition SGS expansion scenario show only moderate heat stress reduction benefits include Oslo, Sarajevo, Murcia, Skopje, or Cluj-Napoca.

We use our results to investigate the amount of increased heat from climate change that may be offset by SGS expansion according to the three SGS scenarios. Figure 7 shows a map of the cities assessed in our studies in terms of the counterbalancing potential (in %) that the *High Ambition* scenario might enable to achieve to contrast the climate change-induced growth (with respect to the current policies climate change scenario) in the daily $T_{wg,\max}$ around 2050. We find that an ambitious but feasibility-constrained scenario of SGS expansion to 2050 could offset 3%–11% [2%–7%] (IQR of the pool of cities assessed) of the projected rise in $T_{wg,max}$ under current policies [SSP5-8.5] (compared to the 2008–2017 climatology). Such range differs when considering different climate metrics and different SGS expansion and climate change scenarios. For example, inaction on SGS could lead to further heat stress due to deteriorating cooling capacity of existing vegetation. We identify Tokyo, Reykjavik, Singapore, Salvador, and Glasgow as the cities where SGS expansion has the largest counterbalancing potential against climate change.

Figure SI-24 shows how a decomposition of the (i) climate change signal and (ii) SGS change signal drivers of change in daily $T_{wg,\max}$ around 2050) for the *High Ambition* SGS scenario and the current policies

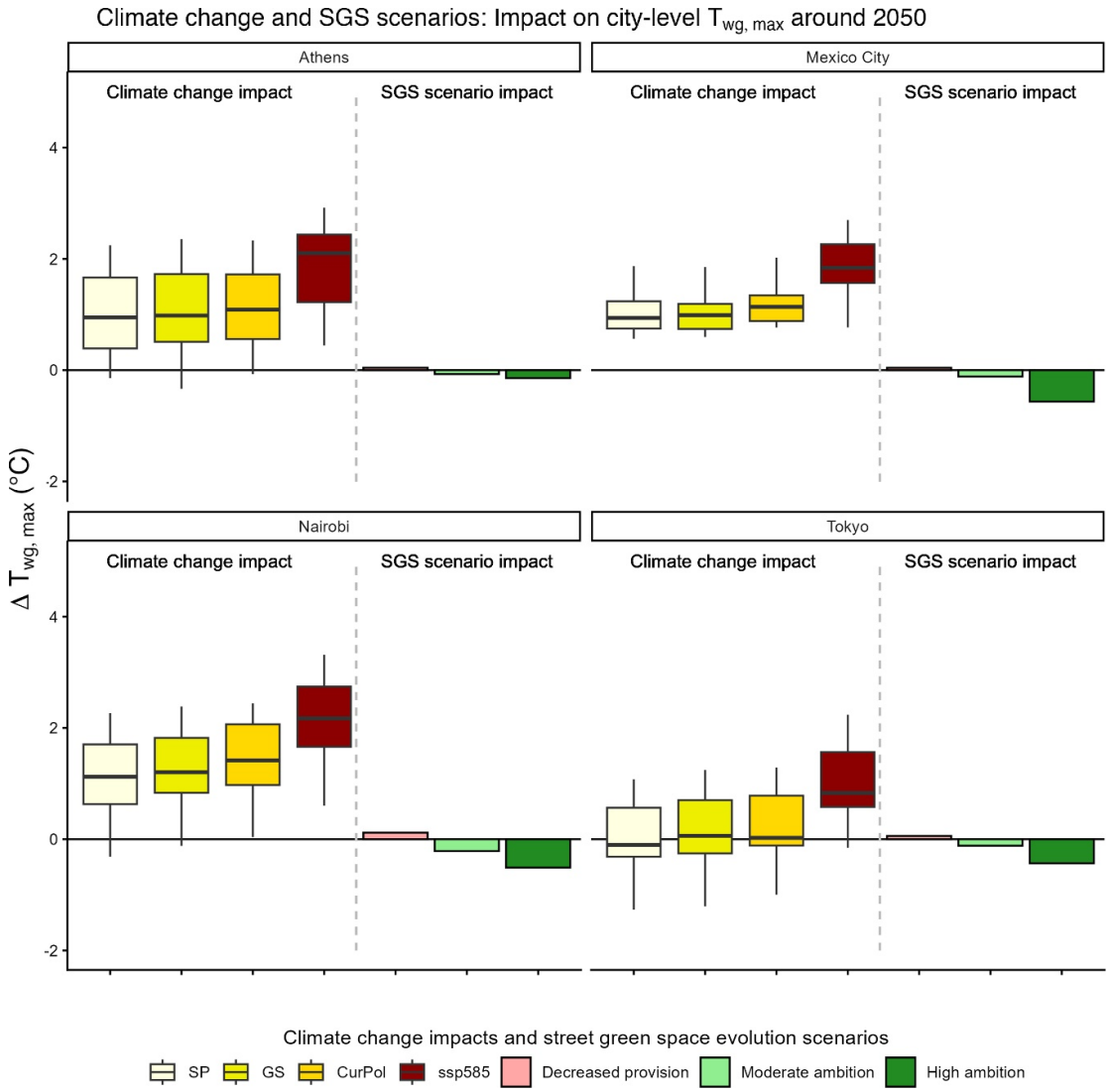

Figure 6. Estimated °C change in daily $T_{wg,max}$ around 2050 in selected cities compared to the 2008-2017 climatology. Whiskers on the left hand-side of each panel show the projected impact of four global climate change scenarios (inclusive of the range of uncertainty from 25 GCMs) from the PROVIDE protocol (Lamboll *et al* 2022) across days of the year; the three bars on the right hand-side of each panel quantify the potential role of street green space evolution scenarios developed and projected in this paper. Each city-level value is obtained as the weighted mean by the change in each LCZ within each city, with the fractions of land area covered by each LCZ class in each city used as weights in the calculation.

climate change scenario around 2050. This additional analysis reveals that for the top five cities by counterbalancing potential, we attribute their rank mostly to their cooling efficiencies estimates being at the upper tail of the distribution across the cities assessed, while for the lowest five the driver is stemming from a more nuanced combination of high expected climate impacts and low effectiveness of street greenery.

4. Discussion

Our study shows that SGS expansion is effective to reduce peak wet-bulb globe temperatures, but it is insufficient as a single strategy to address increasing heat from climate change. Moreover, we demonstrate that the CE of SGS is highly dependent on urban and climate contexts, suggesting that it should not be considered a one-size-fits-all solution. This finding is consistent with recent ultra-local tree evapotranspiration and local microclimate modelling evidence (Gobatti *et al* 2025). As a consequence, city planners should consider SGS as an asset in the urban climate change adaptation portfolio, but not as a panacea against growing urban heat. Keeping a careful eye on within-city distribution of greening to avoid harshening existing climate justice inequalities (Anguelovski *et al* 2019) is important, also noting the large additional range of benefit SGS provides beyond its microclimate regulation function. Moreover, we also highlight that inaction in SGS investment and maintenance could further increase heat stress due to worsening health conditions and lower CE of vegetation.

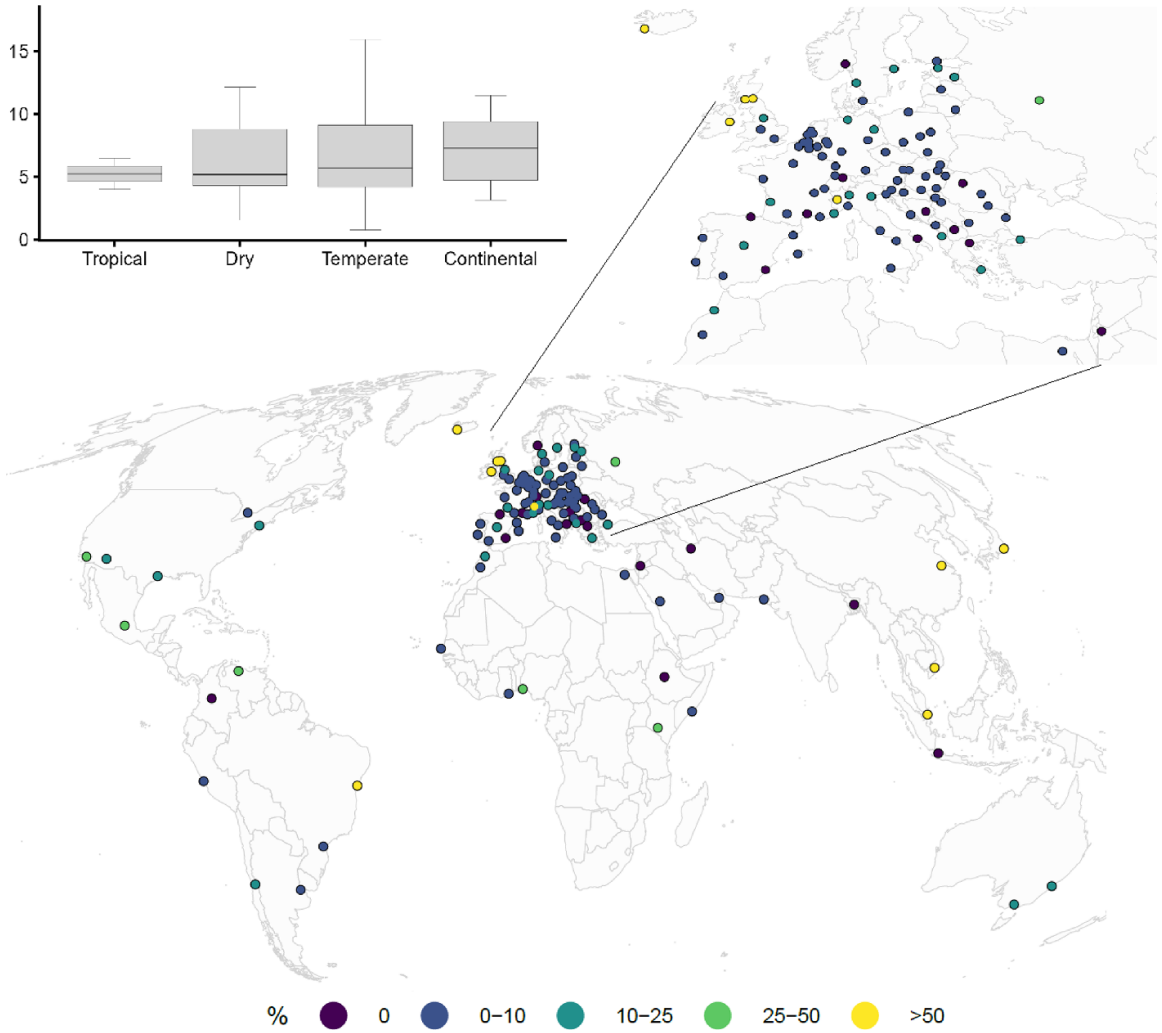

Figure 7. Estimated counterbalancing potential (% of avoided projected climate change impacts on the daily maximum T_{wg} around 2050) for the High ambition SGS scenario against the current policies climate change scenario impact around 2050.

Our results also provide new knowledge about the heterogeneous effectiveness of SGS across climate zones and urban morphology types, underscoring the importance of tailoring adaptation strategies to context-specific realities. The insights provided by our KGC and LCZ-specific results can inform future policies aiming at assessing the city-scale effectiveness of SGS for urban climate adaptation and on the transformation of cities into climate-resilient environments. Such findings can also serve to inform the global discourse on transformative change of cities to achieve both adaptation goals (e.g. by reducing health impacts of urban heat or the risk caused by urban hydrological hazards), as well as energy use reduction and emission mitigation targets (e.g. indoor air cooling energy needs (Meili *et al* 2025)). This is of particular relevance in relation to air-conditioning: although effective in drastically reducing personal indoor exposure (Barreca *et al* 2016, Sera *et al* 2020), it drives energy use and greenhouse gas emissions unless the energy system is decarbonised (Falchetta *et al* 2024). In contrast to urban greening, air-conditioning increases outdoor temperatures (de Munck *et al* 2013, Salamanca *et al* 2014), and it raises climate justice concerns because its ownership and use are highly unequal across socio-economic groups, even within countries, regions, and cities (Pavanello *et al* 2021, Romitti *et al* 2022, Falchetta and Cian 2026).

Despite its innovations, our study holds some key limitations. First, while it would be advantageous to directly model the impact of additional green in an urban climate model, we were not able to follow this approach due to computational and technical constraints. The use of microclimate model outputs present limitations vis-a-vis data collection via local meteorological stations, in particular when using complex heat metrics such as T_{wg}, but allows for a much larger spatial coverage and consistency. The value of the cooling efficiencies reported here reflect the spatial resolution of the climate model (100 m); the larger the resolution of a model, the greater the spatial smoothing of a highly heterogenous temperature field, an intrinsic property of the model output data (Lauwaet *et al* 2024), see also the scaling law identified by Wang *et al* (2024). Therefore, the 100 m resolution captures neighbourhood-scale thermal variability, it does not allow the explicit representation of individual trees or their localised shading and evapotranspiration effects, which are spatially averaged within each grid cell. Hence, CE coefficient estimates should be interpreted as reflecting the average marginal cooling association of SGS at the neighbourhood and LCZ scale, rather than the microclimatic impact of individual trees or specific street segments. Other high-resolution models exist at the CFD-scale, such as PALM (Maronga 2020) or ENVI-MET (ENVI-met GmbH 2022). However, their computational costs limit their application to parts of a city (e.g. Anders and Maronga 2025).

Second, a key concern is residual confounding factors affecting the results of our regression analysis, for example aspects of the built environment and socio-economic sorting that are not fully captured by our controls. Urban geometry may confound SGS-heat relationships beyond what is represented by LCZ classes and average building height: street-canyon aspect ratios, building spacing, orientation relative to prevailing winds, and sky-view factors can alter short-wave and long-wave radiation trapping as well as ventilation, potentially affecting both daytime maxima and nighttime minima, in ways that may either reinforce or offset the association attributed to street greenery. Likewise, surface properties such as pavement and roof materials, albedo, thermal inertia, and maintenance practices (e.g. cool roofs, permeable pavements) may covary with greening intensity and independently influence heat metrics, such that greener streets in better-resourced or recently upgraded areas could exhibit stronger apparent cooling, while greening concentrated in already hot, compact, or poorly ventilated locations could lead to attenuated cooling gradients or even locally positive associations in some urban forms and seasons.

Finally, while our study seeks to contribute to globally-relevant discourses on the systemic role of cities in the climate change debate, the real-world feasibility of the proposed transformations remains a local context-specific matter. Our study attempts to capture feasible SGS transformations by benchmarking the scenarios by observed best cases by climate zone and urban form. However, on specific city-level, other dependencies include factors such as local geography, hydrology, soils, specific urban infrastructures, as well as on governance, financing availability, public acceptance, and last but not least political leadership and willingness for transformation.

Future work might combine a large pool of meteorological station data from a global pool of cities—beyond the limited and Europe-skewed pool covered by the UrbClim model output data used in this paper—to ensure consistency of results when using a wide geographical range of ground truth. Advances in computational power may soon permit Computational Fluid Dynamics-oriented models to run at city-scale while resolving eddies, and ML techniques may also help increase the resolution to include highly-localized cooling effects while allowing to cover entire cities. In addition, future research might evaluate the use of our CE parameter estimates in hydrology and ecology-grounded scenarios of SGS evolution, going beyond the use of the GVI index as a comprehensive but simplified metric of SGS and its canopy coverage. One example are recent studies which evaluates the effect of tree type or species (Pattnaik *et al* 2024), with emerging evidence of

a significant benefit of mixed-species approaches to single ones (Li *et al* 2024a).

5. Conclusion

Irrespective of its limitations, the approach adopted in our research is in line with recent calls by urban climate research for the need to scale down climate and development goals to city-level targets (Bai 2024) and bridge the scale between the local particular and the global universal in climate change assessments of cities (Creutzig *et al* 2025). This is underlined by the upcoming IPCC AR7 *Special Report on Cities and Climate Change*. It is another strong sign of the growing relevance of urban-scale research and efforts to achieve climate action goals. In this context, our paper represents a contribution to the advancement of the understanding of the role of SGS in adapting to increasing heat by using high-granularity urban climate model output (as opposed to the bulk of previous studies, which have used remotely-sensed land-surface temperature), SGS density estimates and implementing such approach to a global pool of cities. The ultimate aim is the development of a set of story-lines and scenarios to project the potential future evolution of SGS and appraise its potential role in reducing local temperature and thus heat-related risk for vulnerable population.

As cities worldwide face higher temperatures, integrating SGS expansion with complementary measures—such as improving building materials and enhancing urban design—will be essential to safeguard public health and liveability, but it does not mean cities can do without continuing efforts to curb anthropogenic greenhouse gas emissions. By providing empirically grounded evidence across a wide global sample of cities, this work highlights both the opportunities and the limits of SGS in adaptation planning, and ultimately calls for holistic, multi-level strategies that combine nature-based solutions with broader systemic climate mitigation and resilience efforts.

Acknowledgments

The authors gratefully acknowledge support from the IIASA 2024 Innovative and Bridging Grant grant URGED (URban mitigation and adaptation strategies Gauging through Empirical functions and Data products) and from the ALPS (ALternative Pathways toward Sustainable development and climate stabilization) sponsored by the Ministry of Economy, Trade and Industry (METI), Japan, and the PROVIDE project, funded by the European Union's Horizon 2020 research and innovation programme under Grant Agreement No. 101003687.

Data availability statement

The data that support the findings of this study are openly available at the following URL/DOI: https://github.com/giacfalk/URGED (Falchetta and Lohrey 2026).

SI Appendix available at https://doi.org/10.1088/1748-9326/ae5c20/data1.

Data and code availability

Computer code to run the analysis and replicate the figures is found at the following repository: https://github.com/giacfalk/URGED. The underlying replication data are hosted on Zenodo in the following repository: https://doi.org/10.5281/zenodo.17803495.

Conflict of interests

The authors declare no competing interest.

Author contributions

Giacomo Falchetta 0000-0003-2607-2195
Conceptualization (lead), Data curation (equal), Formal analysis (equal), Funding acquisition (lead), Investigation (equal), Methodology (equal), Project administration (lead), Resources (equal), Software (equal), Supervision (lead), Validation (equal), Visualization (equal), Writing – original draft (equal), Writing – review & editing (equal)

Steffen Lohrey 0000-0001-7881-9102
Conceptualization (supporting), Data curation (equal), Formal analysis (equal), Investigation (equal), Methodology (equal), Project administration (equal), Resources (equal), Software (equal), Validation (equal), Visualization (equal), Writing – original draft (equal), Writing – review & editing (equal)

Niels Souverijns 0000-0003-4695-9754
Data curation (supporting), Formal analysis (supporting), Investigation (supporting), Methodology (supporting), Writing – original draft (supporting), Writing – review & editing (supporting)

Dirk Lauwaet 0000-0002-9958-5066
Methodology (supporting), Software (supporting), Writing – original draft (supporting), Writing – review & editing (supporting)

Carl-Friedrich Schleussner 0000-0001-8471-848X
Writing – review & editing (supporting)

Leila Niamir 0000-0002-0285-5542
Funding acquisition (supporting), Writing – review & editing (supporting)

References

Amazon Web Services Terrain Tiles 2025 (available at: https://registry.opendata.aws/terrain-tiles) (Accessed on 20 October 2024)

Anders J and Maronga B 2025 Urban microscale simulations based on a Local Climate Zone wizard: Concept and validation using the PALM model system *Urban Clim.* **63** 102576

Anders J, Schubert S, Maronga B and Salim M 2025 Simplifying heat stress assessment: evaluating meteorological variables as single indicators of outdoor thermal comfort in urban environments *Build. Environ.* **274** 112658

Anguelovski I, Connolly J J T, Pearsall H, Shokry G, Checker M, Maantay J, Gould K, Lewis T, Maroko A and Roberts J T 2019 Why green "climate gentrification" threatens poor and vulnerable populations *Proc. Natl Acad. Sci.* **116** 26139–43

Bai X 2024 Post-2030 global goals need explicit targets for cities and businesses *Science* **385** eadq4993

Barreca A, Clay K, Deschenes O, Greenstone M and Shapiro J S 2016 Adapting to climate change: the remarkable decline in the US temperature-mortality relationship over the twentieth century *J. Political Econ.* **124** 105–59

Bowler D E, Buyung-Ali L, Knight T M and Pullin A S 2010 Urban greening to cool towns and cities: a systematic review of the empirical evidence *Landscape Urban Plann.* **97** 147–55

Budd G M 2008 Wet-bulb globe temperature (WBGT)—its history and its limitations *Heat Stress Sport* **11** 20–32

Callaghan A, McCombe G, Harrold A, McMeel C, Mills G, Moore-Cherry N and Cullen W 2021 The impact of green spaces on mental health in urban settings: a scoping review *J. Mental Health* **30** 179–93

Callahan C W 2025 Present and future limits to climate change adaptation *Nat. Sustain.* **8** 336–42

Chakraborty T C, Lee X, Ermida S and Zhan W 2021 On the land emissivity assumption and Landsat-derived surface urban heat islands: a global analysis *Remote Sens. Environ.* **265** 112682

Chan T-C, Lee P-H, Lee Y-T and Tang J-H 2024 Exploring the spatial association between the distribution of temperature and urban morphology with green view index *PLoS One* **19** e0301921

Creutzig F *et al* 2025 Bridging the scale between the local particular and the global universal in climate change assessments of cities *Nat. Cities* **2** 369–78

de León A S G, neda-Gómez A C, Karges N, Leichtle T, Rötzer T, Martin K, Ullmann T and Taubenböck H 2025 The relation of land surface temperature and trees across different urban land use classes based on remote sensing *2025 Joint Urban Remote Sensing Event (JURSE)* vol CFP25RSD-ART pp 1–4

de Munck C, Pigeon G, Masson V, Meunier F, Bousquet P, Tréméac B, Merchat M, Poeuf P and Marchadier C 2013 How much can air conditioning increase air temperatures for a city like Paris, France? *Int. J. Climatol.* **33** 210–27

De Ridder K, Lauwaet D and Maiheu B 2015 UrbClim—a fast urban boundary layer climate model *Urban Clim.* **12** 21–48

Demuzere M, Kittner J, Martilli A, Mills G, Moede C, Stewart I D, Van Vliet J and Bechtel B 2022 A global map of local climate zones to support earth system modelling and urban-scale environmental science *Earth Syst. Sci. Data* **14** 3835–73

Dodman D *et al* 2022 Cities, Settlements and Key Infrastructure *Climate Change 2022: Impacts, Adaptation and Vulnerability. Contribution of Working Group II to the Sixth Assessment Report of the Intergovernmental Panel on Climate Change* ed H-O Pörtner (Cambridge: Cambridge University Press) pp 907–1040

Du M, Li N, Hu T, Yang Q, Chakraborty t T, Venter Z and Yao R 2024 Daytime cooling efficiencies of urban trees derived from land surface temperature are much higher than those for air temperature *Environ. Res. Lett.* **19** 044037

Esperon-Rodriguez M, Gallagher R V, Souverijns N, Lejeune Q, Schleussner C-F and Tjoelker M G 2024 Mapping the climate risk to urban forests at city scale *Landscape Urban Plann.* **248** 105090

European Union Copernicus Land Monitoring Service Information 2022 Water Bodies 2020-present (raster 300 m), global, monthly—version 2 (available at: https://land.copernicus.eu/en/products/water-bodies/water-bodies-global-v2-0-300m) (Accessed 23 June 2024)

Falchetta G and Lohrey S 2026 URban mitigation and adaptation strategies Gauging through Empirical functions and Data products *Github* (available at: https://github.com/giacfalk/URGED)

Falchetta G and Cian E D 2026 *Street Green Space and Electricity Demand: Evidence From Metered Consumption Data in Italy* (Energy Economics)

Falchetta G, Cian E D, Pavanello F and Wing I S 2024 Inequalities in global residential cooling energy use to 2050 *Nat. Commun.* **15** 7874

Falchetta G and Hammad A T 2025 Tracking green space along streets of world cities *Environ. Res.* **5** 025011

Florczyk A *et al* 2019a *GHS-Ucdb R2019a-GHS Urban Centre Database 2015, Multitemporal and Multidimensional Attributes* (European Commission, Joint Research Centre (JRC))

Florczyk A J, Corbane C, Ehrlich D, Freire S, Kemper T, Maffenini L, Melchiorri M, Pesaresi M, Politis P and Schiavina M 2019b GHSL data package 2019 *Luxembourg* **29788** 290498

Friesen J and Taubenböck H 2025 The world's largest cities under climate change and their adaptive capacity to rising heat *Sci. Rep.* **15** 32671

Gasparrini A, Guo Y, Hashizume M, Lavigne E, Zanobetti A, Schwartz J, Tobias A, Tong S, Rocklöv J and Forsberg B 2015 Mortality risk attributable to high and low ambient temperature: a multicountry observational study *Lancet* **386** 369–75

Georgescu M, Morefield P E, Bierwagen B G and Weaver C P 2014 Urban adaptation can roll back warming of emerging megapolitan regions *Proc. Natl Acad. Sci.* **111** 2909–14

Gobatti L, Bach P M, Maurer M and Leitão J P 2025 Impact of soil moisture content on urban tree evaporative cooling and human thermal comfort *npj Urban Sustain.* **5** 1–16

Jiang T, Krayenhoff E S, Martilli A, Nazarian N, Stone B and Voogt J A 2025 Prioritizing urban heat adaptation infrastructure based on multiple outcomes: comfort, health and energy *Proc. Natl Acad. Sci.* **122** e2411144122

Juhola S, Bouwer L M, Huggel C, Mechler R, Muccione V and Wallimann-Helmer I 2024 A new dynamic framework is required to assess adaptation limits *Glob. Environ. Change* **87** 102884

Kirschner V, Macků K, Moravec D and Mañas J 2023 Measuring the relationships between various urban green spaces and local climate zones *Sci. Rep.* **13** 9799

Klimenka M, Zhao K, Hilland R, Zhang F, Voogt J and Ratti C 2025 Instant infrared: estimating urban surface temperatures from street view imagery *Build. Environ.* **267** 112122

Knauer J, El-Madany T S, Zaehle S and Migliavacca M 2018 Bigleaf—An R package for the calculation of physical and physiological ecosystem properties from eddy covariance data *PLoS One* **13** e0201114

Kong Q and Huber M 2022 Explicit calculations of wet-bulb globe temperature compared with approximations and why it matters for labor productivity *Earth's Future* **10** e2021EF002334

Lamboll R, Rogelj J and Schleussner C-F 2022 *A Guide to Scenarios for the Provide Project* (ESS Open Archive)

Lauwaet D, Berckmans J, Hooyberghs H, Wouters H, Driesen G, Lefebre F and De Ridder K 2024 High resolution modelling of the urban heat island of 100 European cities *Urban Clim.* **54** 101850

Lauwaet D, Hooyberghs H, Maiheu B, Lefebvre W, Driesen G, Van Looy S and De Ridder K 2015 Detailed urban heat island projections for cities worldwide: dynamical downscaling cmip5 global climate models *Climate* **3** 391–415

Lee A and Maheswaran R 2011 The health benefits of urban green spaces: a review of the evidence *J. Public Health* **33** 212–22

Li D, Liao W, Rigden A J, Liu X, Wang D, Malyshev S and Shevliakova E 2019 Urban heat island: aerodynamics or imperviousness? *Sci. Adv.* **5** eaau4299

Li G, Cao Y, Fang C, Sun S, Qi W, Wang Z, He S and Yang Z 2025 Global urban greening and its implication for urban heat mitigation *Proc. Natl Acad. Sci.* **122** e2417179122

Li H, Zhao Y, Wang C, Ürge-Vorsatz D, Carmeliet J and Bardhan R 2024a Cooling efficacy of trees across cities is determined by background climate, urban morphology and tree trait *Commun. Earth Environ.* **5** 754

Li Y *et al* 2024b Green spaces provide substantial but unequal urban cooling globally *Nat. Commun.* **15** 7108

Liljegren J C, Carhart R A, Lawday P, Tschopp S and Sharp R 2008 Modeling the wet bulb globe temperature using standard meteorological measurements *J. Occupat. Environ. Hygiene* **5** 645–55

Liu Y, Kwan M-P, Wong M S and Yu C 2023 Current methods for evaluating people's exposure to green space: a scoping review *Soc. Sci. Med.* **338** 116303

Liu Y, Li Q, Yang L, Mu K, Zhang M and Liu J 2020 Urban heat island effects of various urban morphologies under regional climate conditions *Sci. Total Environ.* **743** 140589

Maronga B *et al* 2020 Overview of the PALM model system 6.0 *Geosci. Model Dev.* **13** 1335–72

Massaro E, Schifanella R, Piccardo M, Caporaso L, Taubenböck H, Cescatti A and Duveiller G 2023 Spatially-optimized urban greening for reduction of population exposure to land surface temperature extremes *Nat. Commun.* **14** 2903

Meili N *et al* 2025 Modeling the effect of trees on energy demand for indoor cooling and dehumidification across cities and climates *J. Adv. Model. Earth Syst.* **17** e2024MS004590

Mentaschi L, Duveiller G, Zulian G, Corbane C, Pesaresi M, Maes J, Stocchino A and Feyen L 2022 Global long-term mapping of surface temperature shows intensified intra-city urban heat island extremes *Glob. Environ. Change* **72** 102441

Nutsford D, Pearson A and Kingham S 2013 An ecological study investigating the association between access to urban green space and mental health *Public Health* **127** 1005–11

Oke T R 1982 The energetic basis of the urban heat island *Q. J. R. Meteorol. Soc.* **108** 1–24

Olsson J, Berggren K, Olofsson M and Viklander M 2009 Applying climate model precipitation scenarios for urban hydrological assessment: a case study in Kalmar City *Sweden. 7th Int. Workshop on Precipitation in Urban Areas* vol 92 pp 364–75 (https://doi.org/10.1016/j.atmosres.2009.01.015)

Pattnaik N, Honold M, Franceschi E, Moser-Reischl A, Rıfmmodetextbackslashddototextbackslashelseötextback slashfitzer T, Pretzsch H, Pauleit S and Rahman M A 2024 Growth and cooling potential of urban trees across different levels of imperviousness *J. Environ. Manag.* **361** 121242

Pavanello F, De Cian E, Davide M, Mistry M, Cruz T, Bezerra P, Jagu D, Renner S, Schaeffer R and Lucena A F 2021 Air-conditioning and the adaptation cooling deficit in emerging economies *Nat. Commun.* **12** 6460

Peel M C, Finlayson B L and McMahon T A 2007 Updated world map of the Köppen-Geiger climate classification *Hydrol. Earth Syst. Sci.* **12** 1633–44

Peng S, Piao S, Ciais P, Friedlingstein P, Ottle C, Bréon F-M, Nan H, Zhou L and Myneni R B 2012 Surface urban heat island across 419 global big cities *Environ. Sci. Technol.* **46** 696–703

Puig D, Adger N W, Barnett J, Vanhala L and Boyd E 2025 Improving the effectiveness of climate change adaptation measures *Clim. Change* **178** 7

Rahman M A, Hartmann C, Moser-Reischl A, von Strachwitz M F, Paeth H, Pretzsch H, Pauleit S and Rötzer T 2020 Tree cooling effects and human thermal comfort under contrasting species and sites *Agricultural and Forest Meteorology* **287** 107947

Rocha A D, Vulova S, van der Tol C, Förster Mand Kleinschmit B 2022 Modelling hourly evapotranspiration in urban environments with SCOPE using open remote sensing and meteorological data *Hydrol. Earth Syst. Sci.* **26** 1111–29

Rohat G, Flacke J, Dosio A, Dao H and Maarseveen M 2019 Projections of human exposure to dangerous heat in African Cities under multiple socioeconomic and climate scenarios *Earth's Future* 2018EF001020

Rohat G, Goyette S and Flacke J 2018 Characterization of European cities' climate shift – an exploratory study based on climate analogues *Int. J. Clim. Change Strat. Manag.* **10** 428–52

Romitti Y, Sue Wing I, Spangler K R and Wellenius G A 2022 Inequality in the availability of residential air conditioning across 115 US metropolitan areas *PNAS Nexus* **1** gac210

Salamanca F, Georgescu M, Mahalov A, Moustaoui M and Wang M 2014 Anthropogenic heating of the urban environment due to air conditioning *J. Geophys. Res.: Atmos.* **119** 5949–65

Seiferling I, Naik N, Ratti C and Proulx R 2017 Green streets - Quantifying and mapping urban trees with street-level imagery and computer vision *Landsc. Urban Plan.* **165** 93–101

Sera F, Hashizume M, Honda Y, Lavigne E, Schwartz J, Zanobetti A, Tobias A, niguez I, Vicedo-Cabrera C and Blangiardo M 2020 Air conditioning and heat-related mortality: A multi-country longitudinal study *Epidemiology* **31** 779–87

Shashua-Bar L and Hoffman M 2000 Vegetation as a climatic component in the design of an urban street: an empirical model for predicting the cooling effect of urban green areas with trees *Energy Build.* **31** 221–35

Sinsel T 2022 Advancements and applications of the microclimate model ENVI-met (University of Mainz) (available at: http://www.envi-met.com) (Accessed 13 April 2026)

Souverijns N, Lauwaet D, Lejeune Q, Kropf C M, Yeung K L, Nath S and Schleussner C F 2026 100 m climate and heat stress data up to 2100 for 142 cities around the globe *Data Brief* **65** 112497

Stewart I D and Oke T R 2012 Local climate zones for urban temperature studies *Bull. Am. Meteorol. Soc.* **93** 1879–900

Stull R 2011 Wet-bulb temperature from relative humidity and air temperature *J. Appl. Meteorol. Climatol.* **50** 2267–9

Taubenböck H, Reiter M, Dosch F, Leichtle T, Weigand M and Wurm M 2021 Which city is the greenest? A multi-dimensional deconstruction of city rankings *Comput. Environ. Urban Syst.* **89** 101687

Teeuwen R, Milias V, Bozzon A and Psyllidis A 2024 How well do NDVI and OpenStreetMap data capture people's visual perceptions of urban greenspace? *Landsc. Urban Plan.* **245** 105009

Tran H, Uchihama D, Ochi S and Yasuoka Y 2006 Assessment with satellite data of the urban heat island effects in Asian mega cities *Int. J. Appl. Earth Observat. Geoinform.* **8** 34–48

Turner V K, Middel A and Vanos J K 2023 Shade is an essential solution for hotter cities *Nature* **619** 694–7

Voogt J and Oke T 2003 Thermal remote sensing of urban climates *Remote Sens. Environ.* **86** 370–84

Wang J, Zhou W and Jiao M 2022 Location matters: planting urban trees in the right places improves cooling *Front. Ecol. Environ.* **20** 147–51

Wang J, Zhou W, Jiao M, Zheng Z, Ren T and Zhang Q 2020 Significant effects of ecological context on urban trees' cooling efficiency *ISPRS J. Photogramm. Remote Sens.* **159** 78–89

Wang J, Zhou W, Pickett S T A and Qian Y 2024 A scaling law for predicting urban trees canopy cooling efficiency *Proc. Natl Acad. Sci.* **121** e2401210121

Wang S et al 2025 Dual impact of global urban overheating on mortality *Nat. Clim. Change* **15** 497–504
Willems P and Vrac M 2011 Statistical precipitation downscaling for small-scale hydrological impact investigations of climate change *J. Hydrol.* **402** 193–205
Wong N H, Tan C L, Kolokotsa D D and Takebayashi H 2021 Greenery as a mitigation and adaptation strategy to urban heat *Nat. Rev. Earth Environ.* **2** 166–81
Wu Y et al 2025 Estimating the urban heat-related mortality burden due to greenness: A global modelling study *Lancet Planet. Health* **0** 101235
Xiang Y, Zheng B, Bedra K B, Ouyang Q, Liu J and Zheng J 2023 Spatial and seasonal differences between near surface air temperature and land surface temperature for Urban Heat Island effect assessment *Urban Clim.* **52** 101745
Yaglou C P and Minard D 1957 Control of heat casualties at military training centers *AMA Arch. Indust. Health* **16** 302–16
Zhan W, Wang C, Wang S, Li L, Ji Y, Du H, Huang F, Jiang S, Liu Z and Fu H 2024 Fraction-dependent variations in cooling efficiency of urban trees across global cities *ISPRS J. Photogramm. Remote Sens.* **216** 229–39
Zhou D, Xiao J, Bonafoni S, Berger C, Deilami K, Zhou Y, Frolking S, Yao R, Qiao Z and Sobrino J 2018 Satellite remote sensing of surface urban heat islands: progress, challenges and perspectives *Remote Sens.* **11** 48